Photocatalytic Stability of Single- and Few-Layer MoS_2

Journal:	*ACS Nano*
Manuscript ID	nn-2015-04979t.R1
Manuscript Type:	Article
Date Submitted by the Author:	n/a
Complete List of Authors:	Parzinger, Eric; Technische Universität München, Walter Schottky Institut and Physik-Department; Nanosystems Initiative Munich (NIM), Miller, Bastian; Technische Universität München, Walter Schottky Institut and Physik-Department; Nanosystems Initiative Munich (NIM), Blaschke, Benno; Technische Universität München, Walter Schottky Institut and Physik-Department Garrido, Jose; Technische Universität München, Walter Schottky Institut and Physik-Department Ager, Joel; Lawrence Berkeley National Laboratory, Joint Center for Artificial Photosynthesis Holleitner, Alexander; Technische Universität München, Walter Schottky Institut and Physik-Department; Nanosystems Initiative Munich (NIM), Wurstbauer, Ursula; Technische Universität München, Walter Schottky Institut and Physik-Department; Nanosystems Initiative Munich (NIM),

Photocatalytic Stability of Single- and Few-Layer MoS_2

Eric Parzinger[*,†,‖], *Bastian Miller*[†,‖], *Benno Blaschke*[†], *Jose A. Garrido*[†], *Joel W. Ager*[‡], *Alexander Holleitner*[†,‖] *and Ursula Wurstbauer*[*,†,‖]

[†]Walter Schottky Institut and Physik-Department, Technische Universität München, Am Coulombwall 4a, 85748 Garching, Germany

[‖]Nanosystems Initiative Munich (NIM), Munich 80799, Germany

[‡]Joint Center for Artificial Photosynthesis, Lawrence Berkeley National Laboratory, Berkeley, California 94720, USA

*Address correspondence to eric.parzinger@wsi.tum.de or wurstbauer@wsi.tum.de.

Keywords: Two-dimensional materials, MoS2, Photocatalytic stability, Photocatalytic selectivity, solar water splitting, Raman spectroscopy

ABSTRACT

MoS_2 crystals exhibit excellent catalytic properties and great potential for photo-catalytic production of solar fuel such as hydrogen gas. In this regard, the photocatalytic stability of exfoliated single- and few-layer MoS_2 immersed in water is investigated by μ-Raman spectroscopy. We find that while the basal plane of MoS_2 can be treated as stable under

photocatalytic conditions, the edge sites and presumably also defect sites are highly affected by a photo-induced corrosion process. The edge sites of MoS_2 monolayers are significantly more resistant to photocatalytic degradation compared to MoS_2 multi-layer edge sites. The photo-stability of MoS_2 edge sites depends on the photon energy with respect to the band gap in MoS_2 and also on the presence of oxygen in the electrolyte. These findings are in agreement with an interpretation as oxidation process converting MoS_2 into MoO_x in the presence of oxygen and photo-induced charge carriers. The high stability of the MoS_2 basal plane under photocatalytic treatment with visible light irradiation of extreme light intensities in the order of $P \approx 10 mW/\mu m^2$ substantiates MoS_2's potential as photocatalyst for solar hydrogen production.

MoS_2 is a semiconducting two-dimensional 'van der Waals' material with outstanding electronic,[1,2] optical[3–5] and catalytic[6–8] properties. MoS_2 undergoes a transition from an indirect to a direct band gap semiconductor in the single layer limit[3] with a band gap of $E_{gap} = 1.9$ eV.[4] The high sunlight absorption of up to 10% for atomistic thin layers[9] makes MoS_2 single- but also few-layers a promising material for optoelectronic applications and solar energy harvesting. For pH values between 0 and 7, a single layer of MoS_2 exhibits a suitable band edge alignment with respect to the redox potentials of the hydrogen evolution (H^+/H_2) (HER) and oxygen evolution (O_2/H_2O) (OER) reaction,[10,11] which is an unambiguous requirement of a photo-catalyst for solar driven water splitting with an earth abundant electrolyte such as river or sea water. The peculiarity of MoS_2 is that it holds all requirements for a monolithic device for solar water splitting, because MoS_2 based materials offer not only catalytic activity,[6–8] but also high absorption efficiency in the visible range.[9] The basal planes feature the functionalization as photo absorber, built-in electric fields induced *e.g.* by lateral pn-junctions separate the e-h pairs[12] and the Mo edge along $(10\bar{1}0)$ direction is catalytically active.[13] If a photon is absorbed by an

interband absorption process, the incoming photon promotes an electron from the valence band to the conduction band leaving a hole in the valence band. Such photoexcited electrons can be directly transferred from the conduction band to the energetically preferred potential of the proton reduction. The transferred electron drives the hydrogen evolution reaction. The same applies for the photoexcited holes and the oxygen evolution reaction. Thus, single-layer MoS_2 serves as an ideal candidate for an efficient photocatalyst powering the sunlight-driven photocatalytic water splitting reaction.

Considerable efforts have been made to investigate the catalytic activity of various MoS_2 nanostructures such as nanoparticles,[6,14,15] mesopores,[16] nanowires,[17] amorphous MoS_2,[18–20] thin films[21] and their nanostructure,[13] MoS_2/graphene heterostructures,[22] chemically exfoliated MoS_2 layers,[7,23,24] metal nanoparticle-decorated MoS_2[25] and MoS_2 grown by chemical vapor deposition.[8] Nonetheless, the long term photo-catalytical stability, and not only catalytical stability, is a crucial but often ignored requirement for photo-absorber and catalytic materials in water splitting devices.[26] For electro-catalysts, potential cycling with different scan rates and potential ranges in the dark are the most common methods to address the catalytic stability.[21,22,27] For photocatalytically active materials, however, the catalytic stability in the presence of light irradiation is essential since catalytically stable materials are not per se stable under light irradiation. MoS_2 has been integrated in a silicon tandem photo-electrochemical water splitting device acting as electro-catalyst and simultaneously as corrosion protection for the Si photo-absorber.[28,29] Stability in HER conditions measured by cyclic voltammetry under 1 sun red irradiation ($E_L < 1.95$ eV) has been demonstrated.[28] Bulk and nanostructured MoS_2 materials are efficient and stable photo-cathodes showing sun-light driven HER in a monolithic metal-free

architecture, however progressive photocorrosion under OER conditions limits its functionalization as photoanode because of anodic photo-corrosion along the $\langle 11\bar{2}0 \rangle$ direction.[13]

In this letter, we introduce μ-Raman spectroscopy in aqueous environment to microscopically investigate the stability of well-defined high-quality single- and few-layer MoS_2 crystals under photocatalytic conditions. Of particular interest is the role of the number of layers and hence the impact of the nature of the band gap as well as the role of exciton effects on the stability of the basal plane and edge sites in an earth abundant electrolyte - fresh water. The measurement scheme applies a monochromatic irradiation with high light intensities of $P \approx 10$ mW/μm^2 what would be equivalent to 10^7 suns. Photostability under such challenging conditions certifies a material as durable and can be treated as long-term stable. Long-term stability of MoS_2 in aqueous solutions and in high humidity is not only important for solar-driven water splitting, but also for sensing applications, for functional corrosion protection layer and in general for electronic applications.

Thus, the photo-degradation of MoS_2 flakes immersed in water is *in situ* monitored with a high lateral resolution of about 300 nm and a time resolution of a few seconds. The photo-stability and the evolution of photo-degradation of MoS_2 in presence of water as electrolyte is studied in dependence of crystallographic site, number of layers, energy and intensity of the exposing light as well as the presence of oxygen gas in the electrolyte. We find that the more catalytically active edge sites[30–33] show a much higher photo-degradation compared to the basal plane (a.k.a. terrace sites). We further observe that edge sites of MoS_2 monolayers exhibit a much lower degradation rate compared to edge sites of few-layers with corresponding decay rates of $\tau = 45$ min and $\tau = 1$ min for mono- and bilayer, respectively. Photo-degradation for flakes immersed in water takes place only under irradiation with energy larger than the band-gap of MoS_2. In addition, in our

experiments the presence of oxygen in the electrolyte is required to observe a considerable photo-degradation of the flakes edge sites. Overall, MoS_2 basal planes exhibit superior photo-stability in aqueous environment under extreme irradiation intensities und even the catalytically active edge site are rather stable in the absence of O_2 in the electrolyte.

RESULTS AND DISCUSSION

The investigated MoS_2 flakes are micromechanically exfoliated from bulk crystals and transferred to Si/SiO_2 substrates by a dry stamping technique.[34] The SiO_2 thickness of 275 nm provide an excellent visibility contrast[35,36] so that even single layers of MoS_2 are clearly distinguishable from bi-, tri- and few-layer regions by optical microscopy as well as by monochromatic reflectivity measurements. The samples are characterized prior and after the photocatalytic degradation studies by a set of microscopy and spectroscopy tools under ambient conditions. Size and changes in geometry are investigated by contrast images from optical microscopy, and monochromatic reflectivity measurements by scanning a laser with low power and high sampling rate over the sample and recording the reflected light with a photo-diode. The morphology is investigated by atomic force microscopy. From spatially resolved Raman spectroscopy, we gain access to various parameters such as the number of layers,[37] doping level[38] and even the presence of adsorbates.[39] Furthermore, the degradation process is monitored *in situ* by real-time Raman spectroscopy utilizing the irradiation laser of the photo-degradation studies for the Raman measurements. The most important figure of merits in the presented experiments is the time evolution of the phonon-mode energies as fingerprint for the number of layers and the change in the integrated intensity of the individual modes as sensor for the amount of unaffected and not photo-degraded crystalline volume. A high spatial resolution for all optical measurements in liquid is realized through a laser spot size of about 300 nm given by a water-

dipping objective and mounting the sample on *x*-*y*-*z* piezo scanner. If not stated otherwise, deionized (DI) water is used as electrolyte.

Figure 1 demonstrates the photo-stability of a mono-/trilayer flake under irradiation with a focused laser with energy E_{laser} = 2.54 eV. This energy is larger than the band-gap of MoS_2 (E_{gap} = 1.9eV). The region of interest (ROI) is marked on the optical microscopy image in Figure 1(a). The laser is scanned across a field consisting of monolayer (1L) and trilayer (3L) parts along the path shown on the reflectivity image in Figure 1(b) (on the right). The laser with a power of P_{laser} = 1 mW is kept at each spot for 20 s, and the step size during the scanning process is 250 nm. The sample is completely immersed in DI water during the whole scan. Figure 1(b) shows the reflectivity image taken prior (left side) and after exposure to laser light (right side). The right side discloses that the whole scanned 3L region is thinned down, whereas part of the 1L region seems to be unaffected. Other parts of the monolayer region are missing. In a next step, Raman measurements in ambient conditions are recorded on several positions on the MoS_2 flake [Figure 1(c)]: untreated 3L region (♦), thinned 3L region (▲), affected 1L (●) and untreated 1L region (■). The two characteristic zone-center phonons of MoS_2 are observable in the spectra. The E^1_{2g} mode is an in-plane mode, with the atoms oscillating parallel to the basal plane and the A_{1g} mode is an out-of-plane oscillation with the sulfur atoms oscillating in opposite direction as sketched in Figure 2. The Raman measurements confirm the observation already seen from the reflectivity measurements. The Raman spectrum within the thinned area (▲) matches that of a monolayer, except a slight shift of the A_{1g} mode towards higher wavenumbers. This upshift in energy of ~0.3 cm^{-1} can be explained by a decreased charge carrier density, consistent with an increased number of adsorbed molecules on defect sites.[39–41] The reminiscent weak Raman intensities at the degraded monolayer region (●) is either attributed to a diluted amount of residual MoS_2

nanoflakes or to the fact that the spatial resolution of the water dipping objective is decreased by the measurements without liquid. The Raman spectra further demonstrate that the non-exposed 3L (♦) and 1L areas (■) are unaffected and consequently stable in water without illumination.

To study the photo-corrosion process in more detail, we repeatedly record Raman spectra on a different sample with bi-layer MoS_2 edges as well as basal planes. Again, the excitation energy is chosen to be above the band gap (E_{laser} = 2.54 eV). The measurements are carried out for various light intensities on various spots containing edge or terrace sites exemplarily demonstrated on the flake shown in Figure 2(a). The temporal evolution of energy as well as intensity of the two relevant phonon modes A_{1g} and E^1_{2g}, whose oscillation schemes are sketched in Figure 2(b), enable us to *in situ* monitor the photo-induced degradation process with a high spatial resolution by Raman scattering. Figures 2(c) and (d) depict the temporal evolution of the integrated intensities of the phonon modes recorded on the edge sites marked in Figure 2(a) for different light intensities. For clarity and better comparability, the peaks are normalized to their initial intensity. The related Raman spectra are plotted in Figure 2(e) for t = 0 sec (◊) and in Figure 2(f) after $t \approx 1$ min (○). At the beginning of the measurement (t = 0 sec) marked by (◊) in Figures 2(c,d), the energies of the relevant phonon modes are unambiguously corresponding to those of bi-layer MoS_2 [Figure 2(e)]. After approximately 1 minute, marked by (○) in panels (c,d), the signal of both Raman modes drop to about 50% of the initial intensities. Simultaneously, the E^1_{2g} Raman mode is blue-shifted and the A_{1g} Raman mode is redshifted. This change in the photon energies definitely marks the transition from a MoS_2 bi-layer to a MoS_2 monolayer[37] after ~1 min of light exposure [Figure 2(f)]. The photo-induced transition from bi- to monolayer MoS_2 is in line with the fact that the recorded Raman signals of both phonon modes disclose two distinct degradation rates. These rates exhibit an exponential decay rate of $\tau \approx 1$ min and $\tau \approx 45$ min,

respectively. Therefore, the initial fast decay rate can be interpreted as the stability of the bi-layer edge site, whereas the much slower decay rate is the stability of the monolayer. For comparison, Figure 2(g) depicts the temporal evolution of the normalized integrated intensity of the silicon TO-phonon mode. The intensity of the Si-phonon mode increases by a similar amount as the intensity of the two MoS_2-phonon modes decreases approaching the intensity value of the Si-mode on the pristine substrate. This opposite trend of the intensities of Si and MoS_2 phonon modes, respectively, corroborates the above given interpretation that the drop in intensity of the Raman modes of the photo-excited MoS_2 is because of photo-degradation of the material and that it is not caused by spurious effects like the loss of laser focus. The overall exponential decay is power independent between 0.5 mW and 1.5 mW [Figures 2(c) and (d)]. This is interpreted such that the corrosion process is already saturated with a laser power of 0.5 mW. The photo-degradation is most likely limited by a rather slow oxidation rate linked to the density of mobile holes η_{fh} in MoS_2, but not directly linked to the absolute density of photo-excited charge carriers η and the oxidation rate is presumably also affected by the diffusion of reactive species present in the electrolyte. The rate is expected to be slower than the turn over frequency (TOF) for the HER reported to be TOF = 0.02 s^{-1} per MoS_2 edge site.[30] The density of photo-induced e-h pairs constitutes approximately $\eta > 10^{11}$ cm^{-2} for a spot diameter of ~300 nm, laser wavelength of 488 nm, an absorption efficiency of ~ 10% and an e-h recombination slower than 1 ps.[42] The number of freely mobile holes η_{fh} is expected to be larger for the bilayer because of the combined effect of a reduced exciton binding energy from 0.64 eV[43] for the monolayer to less than 0.21 eV (number for $MoSe_2$, similar value expected for MoS_2)[44] for bilayers and by an increased lifetime of the holes as expected for an indirect bandgap semiconductors.

We now reveal the role of number of layers as well as the difference between edge and terrace sites for the photo-corrosion process. We illuminate several MoS_2 samples consisting of mono- and few-layer regions with three different geometries: either scanning the laser across a field on the sample in a specific pattern as shown *e.g.* in Figure 1, illuminating a spot either on the samples' edge or basal plane (see Figure 2) or scanning the laser along a line from the substrate onto the flake across steps from mono- to multilayer region or *vice versa* and back from the flake to the substrate as demonstrated on the MoS_2 flake in Figure 3.

Figure 3 depicts an optical micrograph and an atomic force microscopy (AFM) image with corresponding height profile before and after a laser line scan from the substrate across a trilayer to a protruding monolayer area. The transition from substrate over the edge of the trilayer region is marked as (1), the transition from trilayer to the protruding monolayer with (2) and over the monolayer edge site to the substrate with (3). The laser scan is performed with the sample immersed in DI water, a laser excitation energy of 2.54 eV (488 nm), a step size of 100 nm and a dose of 200 μW x 120 s at each spot. The removal of the trilayer part starting at the edge site (1) is clearly visible, while the single layer seems almost unaffected as evident in the AFM height profiles perpendicular to the line of the laser scan. The monolayer seems to be undamaged at transition (2) from tri- to monolayer without hitting a monolayer edge and is visibly only affected at the step (3) from the monolayer region to the substrate. This linescan shows that the edge sites are degraded after illumination in water, whereas the basal plane remains visibly unaffected in agreement with the previous reported findings.

Focusing the laser on a single spot on the basal plane of a trilayer yields no corrosion of the flake on a similar timescale and irradiation dose. Such a difference in the photo-degradation between edge and basal plane has been observed for all investigated flakes. The terrace site can

be treated as stable under the assumption that the photo-corrosion observed *e.g.* in Figure 1 on the 1L part starts on defect sites. Like edge sites, defect sites imply dangling bonds that are expected to be responsible for the enlarged catalytic activity compared to the basal plane. The absence of dangling bonds at the basal planes is characteristic for van-der Waals layered materials such as MoS_2.

We find that the photo-excitation of electron-hole pairs is essential for the photo-degradation process. The MoS_2 edge sites only degrade under light exposure with energies larger than the band gap. Figure 4 contrasts two optical images of the same flake after laser scans conducted with an energy of E_{laser} = 1.59 eV and E_{laser} = 2.54 eV, corresponding to illumination with energy smaller and larger than the direct band gap of MoS_2, respectively. For the lower irradiation energy, no corrosion shows up neither on the MoS_2 edge nor on the illuminated basal planes (laser power P_{laser} = 1.5 W). The complementary scan with light energy of 2.54 eV (P_{laser} = 0.5 W), however, clearly displays a decomposition of the flake over a large area. From the scan direction of the laser, marked by the arrows in Figure 4, we again see that the photo-degradation predominantly starts at the step-edges of the individual planes.

Let us now turn to the role of reactive species in the electrolyte. The power-independence of the photo-degradation rate [Figure 2(e) and (f)] points already towards the importance of reactive species and their amount on the interface between MoS_2 and electrolyte. Their role is investigated on example of oxygen as reactive species by changing the amount of dissolved oxygen in the DI water. To this end, the photo-stability of edge sites of a bi-layer flake immersed in degased DI water is studied with parameters similar to those shown in Figure 2. The DI water is degased with inert nitrogen gas in order to reduce the amount of naturally dissolved oxygen. The photo-degradation rates of MoS_2 bilayers immersed in water with and without oxygen are

compared in Figure 5. The drop in the MoS_2 Raman intensities monitoring the degradation is indeed significantly reduced, when the sample is immersed in water with a strongly reduced oxygen concentration. The remaining degradation rate might be influenced by the steadily increasing oxygen content in the DI water over time. During the measurements, the surface of the water basin is in contact to ambient air and consequently it is expected that the nitrogen gas dissolved in the electrolyte is again replaced by oxygen gas.

Overall, all our observations are in agreement with the interpretation that MoS_2 terrace sites immersed in water as electrolyte can be treated as stable under photocatalytic conditions even under extreme irradiation intensity of 10 $mW/\mu m^2$. Edges and presumably also defects sites, however, exhibit a significant, photo-generated charge carrier driven catalytic degradation in the presence of reactive species such as oxygen. Opposite to reported laser thinning, where thermal ablation caused by laser heating is used to thin MoS_2 to monolayers,[45] the process reported here is of significant different origin. Thermal ablation causes are unlikely to produce the observed photodegradation because of the low laser power, absence of a power dependence, the distinct difference between edge sites and basal plane and also the absence of degradation for light energy below the band gap. We propose a charge carrier driven photo-catalytic oxidation process converting MoS_2 into MoO_3 or more general into MoO_x as the underlying process for the photo-degradation. The MoO_x then dissolves in the electrolyte[8] in agreement with the absence of any MoO_x signatures in a suitable energy range in Raman spectroscopy. This photo-corrosion process is believed to be responsible for the photo-degradation of MoS_2 at area-scans, line-scans as well as spot-like exposure of edge sites with light above the band-gap. The amount of dissolved MoO_x in the electrolyte from a 1 µm x 1 µm oxidized area of a flake would result in approximately 10^{-14} g of MoO_x in more than 1 ml water in a petri dish that is not sealed against

the environment. For this reason it is not possible in this study to further investigate the MoO_x compound *e.g.* by inductively coupled plasma mass spectrometry.

The fact that we observe photo-corrosion predominantly on edge sites can be explained by a more favored transfer of charge carriers to the electrolyte from edge and defect sites due to existent dangling bonds compared to the basal plane without dangling bonds. The found degradation on some individual spots on the basal plane suggest to start at lattice defects. Such individual defects of the crystal are beyond the resolution in our experiments and therefore we can only conjecture about the role of defect sites. The observed layer dependence is interpreted in terms of an increased density of freely mobile holes η_{fh} for MoS_2 bi- and multilayers compared to the monolayer because of a much larger exciton-binding energy for the monolayer resulting in a reduced e-h separation efficiency. The observed layer dependence might be further amplified by an increased life-time of photo-generated charge carriers due to the reduced recombination rate for the indirect band-gap of MoS_2 bi-, tri- and multilayers compared to the direct band gap in the monolayer limit. A role of the supporting substrate is unlikely since we assume a thin water layer between the MoS_2 flake and the hydrophilic SiO_2 substrates as the exfoliation process has not been done in inert atmosphere. This assumption is supported by atomic force microscopy height profile revealing a step height from substrate to MoS_2 monolayer of about 3 nm, whereas the step height from monolayer to bilayer constitutes 0.7 nm close to the theoretical value.

CONCLUSION

In summary, we find that the MoS_2 edge sites are subject to significant photo-corrosion under light exposure with a laser energy larger than the direct band gap, when immersed in an

electrolyte with dissolved oxygen. The photo-corrosion process is found to take place on edge and most likely also defect sites. The photo-degradation rate is much faster for bi- and multi-layer ($\tau_1 \sim 1$ min) compared to monolayer ($\tau_2 \sim 45$ min) MoS_2 and is explained by the transition from an indirect to a direct semiconductor resulting in an decreased amount of freely mobile photogenerated holes η_{fh} due to an increased exciton binding energy and reduced lifetime of the charge carriers. The degradation process is interpreted in terms of an oxidation process driven by the photo-generated charge carriers converting MoS_2 *e.g.* into MoO_x that is expected to be dissolved in the electrolyte. The role of photo-generated charge carriers as driving force can explain the layer-dependence as well as the superior catalytic degradation of the edges compared to basal planes.

The MoS_2 basal plane is found to exhibit a high level of photocatalytic stability even in the presence of reactive species such as oxygen in the electrolyte and under irradiation with visible light of intensities exceeding 10 mW/μm^2. The stability in photocatalytic conditions is an unambiguous requirement of a photo-absorber for photocatalytic splitting of water, but also for sensing applications, transparent corrosion protection layer with further functionality and general for optoelectronic device applications in aqueous or humid environment. The stability under challenging conditions together with high absorption in the visible range and the electro-catalytic activity strengthen MoS_2's potential for sunlight driven overall hydrogen production by water splitting in a durable monolithic device without any metals utilizing the earth abundant electrolyte fresh water.

METHODS

MoS_2 flakes are prepared by standard micromechanical exfoliation from bulk crystal (SPI supplies) and then transferred to a p-type doped Si substrate with a 275 nm thick thermal oxide layer on top. The transfer is accomplished by an all-dry viscoelastic stamping technique[34] using a polydimethylsiloxane (PDMS) thin film. The flakes are investigated by optical contrast, scanning reflectivity measurements, atomic force microscopy as well as Raman spectroscopy.

All optical measurements, reflectivity scans as well as μ-Raman spectroscopy and laser cutting with the sample immersed in the electrolyte are performed using a 63x water immersion objective (Carl Zeiss Objective W N-Achroplan 63x/0.9 M27) in combination with a piezo stack with a closed-loop resolution of 1 nm (Physik Instrumente P-611.3 NanoCube® XYZ-System). This combination allows us to reach a spatial resolution of roughly 300 nm in our measurements with the sample in the electrolyte. The position of the flake is monitored before and after each measurement in order to exclude any influence due to lateral drifts. Laser excitation energies below (λ = 780 nm) and above the direct band gap energy (λ = 488 nm) are accessed utilizing a Ti:Saphire and Ar-ion gas laser, respectively, as excitation light source.

AUTHOR INFORMATION

Corresponding Author

*E-Mail: eric.parzinger@wsi.tum.de (E.P.).

*E-Mail: ursula.wurstbauer@wsi.tum.de (U.W).

Author Contributions

The manuscript was written through contributions of all authors. All authors have given approval to the final version of the manuscript.

Funding Sources

We acknowledge financial support by the DFG *via* excellence cluster Nanosystems Initiative Munich (NIM) and project Ho 3324/8-1 as well as BaCaTeC.

ABBREVIATIONS

HER, hydrogen evolution reaction; OER, oxygen evolution reaction; e-h, electron-hole; DI, deionized; atomic force microscopy (AFM);

REFERENCES

1. Radisavljevic, B.; Radenovic, A.; Brivio, J.; Giacometti, V.; Kis, A. Single-Layer MoS_2 Transistors. *Nat. Nanotechnol.* **2011**, *6*, 147–150.

2. Wang, Q. H.; Kalantar-Zadeh, K.; Kis, A.; Coleman, J. N.; Strano, M. S. Electronics and Optoelectronics of Two-Dimensional Transition Metal Dichalcogenides. *Nat. Nanotechnol.* **2012**, *7*, 699–712.

3. Splendiani, A.; Sun, L.; Zhang, Y.; Li, T.; Kim, J.; Chim, C.-Y.; Galli, G.; Wang, F. Emerging Photoluminescence in Monolayer MoS_2. *Nano Lett.* **2010**, *10*, 1271–1275.

4. Mak, K. F.; Lee, C.; Hone, J.; Shan, J.; Heinz, T. F. Atomically Thin MoS_2: A New Direct-Gap Semiconductor. *Phys. Rev. Lett.* **2010**, *105*, 136805.

5. Mak, K. F.; He, K.; Shan, J.; Heinz, T. F. Control of Valley Polarization in Monolayer MoS_2 by Optical Helicity. *Nat. Nanotechnol.* **2012**, *7*, 494–498.

6. Hinnemann, B.; Moses, P. G.; Bonde, J.; Jørgensen, K. P.; Nielsen, J. H.; Horch, S.; Chorkendorff, I.; Nørskov, J. K. Biomimetic Hydrogen Evolution: MoS_2 Nanoparticles as Catalyst for Hydrogen Evolution. *J. Am. Chem. Soc.* **2005**, *127*, 5308–5309.

7. Chhowalla, M.; Shin, H. S.; Eda, G.; Li, L.-J.; Loh, K. P.; Zhang, H. The Chemistry of Two-Dimensional Layered Transition Metal Dichalcogenide Nanosheets. *Nat. Chem.* **2013**, *5*, 263–275.

8. Yu, Y.; Huang, S.-Y.; Li, Y.; Steinmann, S. N.; Yang, W.; Cao, L. Layer-Dependent Electrocatalysis of MoS_2 for Hydrogen Evolution. *Nano Lett.* **2014**, *14*, 553–558.

9. Bernardi, M.; Palummo, M.; Grossman, J. C. Extraordinary Sunlight Absorption and One Nanometer Thick Photovoltaics Using Two-Dimensional Monolayer Materials. *Nano Lett.* **2013**, *13*, 3664–3670.

10. Li, Y.; Li, Y.-L.; Araujo, C. M.; Luo, W.; Ahuja, R. Single-Layer MoS_2 as an Efficient Photocatalyst. *Catal. Sci. Technol.* **2013**, *3*, 2214–2220.

11. Zhuang, H. L.; Hennig, R. G. Computational Search for Single-Layer Transition-Metal Dichalcogenide Photocatalysts. *J. Phys. Chem. C* **2013**, *117*, 20440–20445.

12. Choi, M. S.; Qu, D.; Lee, D.; Liu, X.; Watanabe, K.; Taniguchi, T.; Yoo, W. J. Lateral MoS_2 P–n Junction Formed by Chemical Doping for Use in High-Performance Optoelectronics. *ACS Nano* **2014**, *8*, 9332–9340.

13. Chen, Z.; Forman, A. J.; Jaramillo, T. F. Bridging the Gap Between Bulk and Nanostructured Photoelectrodes: The Impact of Surface States on the Electrocatalytic and Photoelectrochemical Properties of MoS_2. *J. Phys. Chem. C* **2013**, *117*, 9713–9722.

14. Bonde, J.; Moses, P. G.; Jaramillo, T. F.; Nørskov, J. K.; Chorkendorff, I. Hydrogen Evolution on Nano-Particulate Transition Metal Sulfides. *Faraday Discuss.* **2008**, *140*, 219–231.

15. Vrubel, H.; Merki, D.; Hu, X. Hydrogen Evolution Catalyzed by MoS_3 and MoS_2 Particles. *Energy Environ. Sci.* **2012**, *5*, 6136–6144.

16. Kibsgaard, J.; Chen, Z.; Reinecke, B. N.; Jaramillo, T. F. Engineering the Surface Structure of MoS_2 to Preferentially Expose Active Edge Sites for Electrocatalysis. *Nat. Mater.* **2012**, *11*, 963–969.

17. Chen, Z.; Cummins, D.; Reinecke, B. N.; Clark, E.; Sunkara, M. K.; Jaramillo, T. F. Core–shell MoO_3–MoS_2 Nanowires for Hydrogen Evolution: A Functional Design for Electrocatalytic Materials. *Nano Lett.* **2011**, *11*, 4168–4175.

18. Merki, D.; Fierro, S.; Vrubel, H.; Hu, X. Amorphous Molybdenum Sulfide Films as Catalysts for Electrochemical Hydrogen Production in Water. *Chem. Sci.* **2011**, *2*, 1262–1267.

19. Benck, J. D.; Chen, Z.; Kuritzky, L. Y.; Forman, A. J.; Jaramillo, T. F. Amorphous Molybdenum Sulfide Catalysts for Electrochemical Hydrogen Production: Insights into the Origin of Their Catalytic Activity. *ACS Catal.* **2012**, *2*, 1916–1923.

20. Shin, S.; Jin, Z.; Kwon, D. H.; Bose, R.; Min, Y.-S. High Turnover Frequency of Hydrogen Evolution Reaction on Amorphous MoS_2 Thin Film Directly Grown by Atomic Layer Deposition. *Langmuir* **2015**, *31*, 1196–1202.

21. Kong, D.; Wang, H.; Cha, J. J.; Pasta, M.; Koski, K. J.; Yao, J.; Cui, Y. Synthesis of MoS_2 and $MoSe_2$ Films with Vertically Aligned Layers. *Nano Lett.* **2013**, *13*, 1341–1347.

22. Li, Y.; Wang, H.; Xie, L.; Liang, Y.; Hong, G.; Dai, H. MoS_2 Nanoparticles Grown on Graphene: An Advanced Catalyst for the Hydrogen Evolution Reaction. *J. Am. Chem. Soc.* **2011**, *133*, 7296–7299.

23. Lukowski, M. A.; Daniel, A. S.; Meng, F.; Forticaux, A.; Li, L.; Jin, S. Enhanced Hydrogen Evolution Catalysis from Chemically Exfoliated Metallic MoS_2 Nanosheets. *J. Am. Chem. Soc.* **2013**, *135*, 10274–10277.

24. Voiry, D.; Yamaguchi, H.; Li, J.; Silva, R.; Alves, D. C. B.; Fujita, T.; Chen, M.; Asefa, T.; Shenoy, V. B.; Eda, G.; *et al.* Enhanced Catalytic Activity in Strained Chemically Exfoliated WS_2 Nanosheets for Hydrogen Evolution. *Nat. Mater.* **2013**, *12*, 850–855.

25. Kang, Y.; Gong, Y.; Hu, Z.; Li, Z.; Qiu, Z.; Zhu, X.; Ajayan, P. M.; Fang, Z. Plasmonic Hot Electron Enhanced MoS_2 Photocatalysis in Hydrogen Evolution. *Nanoscale* **2015**, *7*, 4482–4488.

26. Benck, J. D.; Hellstern, T. R.; Kibsgaard, J.; Chakthranont, P.; Jaramillo, T. F. Catalyzing the Hydrogen Evolution Reaction (HER) with Molybdenum Sulfide Nanomaterials. *ACS Catal.* **2014**, *4*, 3957–3971.

27. Wang, T.; Liu, L.; Zhu, Z.; Papakonstantinou, P.; Hu, J.; Liu, H.; Li, M. Enhanced Electrocatalytic Activity for Hydrogen Evolution Reaction from Self-Assembled Monodispersed Molybdenum Sulfide Nanoparticles on an Au Electrode. *Energy Environ. Sci.* **2013**, *6*, 625–633.

28. Laursen, A. B.; Pedersen, T.; Malacrida, P.; Seger, B.; Hansen, O.; Vesborg, P. C. K.; Chorkendorff, I. MoS_2—an Integrated Protective and Active Layer on N^+p-Si for Solar H_2 Evolution. *Phys. Chem. Chem. Phys.* **2013**, *15*, 20000–20004.

29. Benck, J. D.; Lee, S. C.; Fong, K. D.; Kibsgaard, J.; Sinclair, R.; Jaramillo, T. F. Designing Active and Stable Silicon Photocathodes for Solar Hydrogen Production Using Molybdenum Sulfide Nanomaterials. *Adv. Energy Mater.* **2014**, *4*, 1400739.

30. Jaramillo, T. F.; Jørgensen, K. P.; Bonde, J.; Nielsen, J. H.; Horch, S.; Chorkendorff, I. Identification of Active Edge Sites for Electrochemical H_2 Evolution from MoS_2 Nanocatalysts. *Science* **2007**, *317*, 100–102.

31. Wang, H.; Zhang, Q.; Yao, H.; Liang, Z.; Lee, H.-W.; Hsu, P.-C.; Zheng, G.; Cui, Y. High Electrochemical Selectivity of Edge versus Terrace Sites in Two-Dimensional Layered MoS2 Materials. *Nano Lett.* **2014**, *14*, 7138–7144.

32. Benson, J.; Li, M.; Wang, S.; Wang, P.; Papakonstantinou, P. Electrocatalytic Hydrogen Evolution Reaction on Edges of a Few Layer Molybdenum Disulfide Nanodots. *ACS Appl. Mater. Interfaces* **2015**, *7*, 14113–14122.

33. Tsai, C.; Chan, K.; Abild-Pedersen, F.; Nørskov, J. K. Active Edge Sites in $MoSe_2$ and WSe_2 Catalysts for the Hydrogen Evolution Reaction: A Density Functional Study. *Phys. Chem. Chem. Phys.* **2014**, *16*, 13156–13164.

34. Castellanos-Gomez, A.; Buscema, M.; Molenaar, R.; Singh, V.; Janssen, L.; Zant, H. S. J. van der; Steele, G. A. Deterministic Transfer of Two-Dimensional Materials by All-Dry Viscoelastic Stamping. *2D Mater.* **2014**, *1*, 011002.

35. Castellanos-Gomez, A.; Agraït, N.; Rubio-Bollinger, G. Optical Identification of Atomically Thin Dichalcogenide Crystals. *Appl. Phys. Lett.* **2010**, *96*, 213116.

36. Benameur, M. M.; Radisavljevic, B.; Héron, J. S.; Sahoo, S.; Berger, H.; Kis, A. Visibility of Dichalcogenide Nanolayers. *Nanotechnology* **2011**, *22*, 125706.

37. Lee, C.; Yan, H.; Brus, L. E.; Heinz, T. F.; Hone, J.; Ryu, S. Anomalous Lattice Vibrations of Single- and Few-Layer MoS_2. *ACS Nano* **2010**, *4*, 2695–2700.

38. Chakraborty, B.; Bera, A.; Muthu, D. V. S.; Bhowmick, S.; Waghmare, U. V.; Sood, A. K. Symmetry-Dependent Phonon Renormalization in Monolayer MoS_2 Transistor. *Phys. Rev. B* **2012**, *85*, 161403.

39. Miller, B.; Parzinger, E.; Vernickel, A.; Holleitner, A. W.; Wurstbauer, U. Photogating of Mono- and Few-Layer MoS_2. *Appl. Phys. Lett.* **2015**, *106*, 122103.

40. Tongay, S.; Zhou, J.; Ataca, C.; Liu, J.; Kang, J. S.; Matthews, T. S.; You, L.; Li, J.; Grossman, J. C.; Wu, J. Broad-Range Modulation of Light Emission in Two-Dimensional Semiconductors by Molecular Physisorption Gating. *Nano Lett.* **2013**, *13*, 2831–2836.

41. Nan, H.; Wang, Z.; Wang, W.; Liang, Z.; Lu, Y.; Chen, Q.; He, D.; Tan, P.; Miao, F.; Wang, X.; *et al.* Strong Photoluminescence Enhancement of MoS_2 through Defect Engineering and Oxygen Bonding. *ACS Nano* **2014**, *8*, 5738–5745.

42. Shi, H.; Yan, R.; Bertolazzi, S.; Brivio, J.; Gao, B.; Kis, A.; Jena, D.; Xing, H. G.; Huang, L. Exciton Dynamics in Suspended Monolayer and Few-Layer MoS2 2D Crystals. *ACS Nano* **2013**, *7*, 1072–1080.

43. Hill, H. M.; Rigosi, A. F.; Roquelet, C.; Chernikov, A.; Berkelbach, T. C.; Reichman, D. R.; Hybertsen, M. S.; Brus, L. E.; Heinz, T. F. Observation of Excitonic Rydberg States in Monolayer MoS_2 and WS_2 by Photoluminescence Excitation Spectroscopy. *Nano Lett.* **2015**, *15*, 2992–2997.

44. Liu, H. J.; Jiao, L.; Xie, L.; Yang, F.; Chen, J. L.; Ho, W. K.; Gao, C. L.; Jia, J. F.; Cui, X. D.; Xie, M. H. Molecular-Beam Epitaxy of Monolayer and Bilayer WSe_2 : A Scanning Tunneling Microscopy/spectroscopy Study and Deduction of Exciton Binding Energy. *2D Mater.* **2015**, *2*, 034004.

45. Castellanos-Gomez, A.; Barkelid, M.; Goossens, A. M.; Calado, V. E.; van der Zant, H. S. J.; Steele, G. A. Laser-Thinning of MoS_2: On Demand Generation of a Single-Layer Semiconductor. *Nano Lett.* **2012**, *12*, 3187–3192.

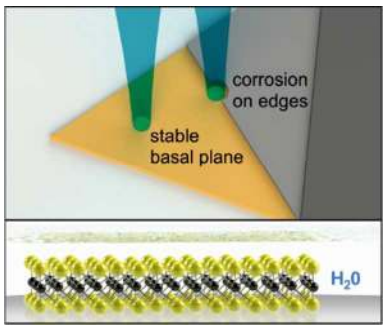

TOC

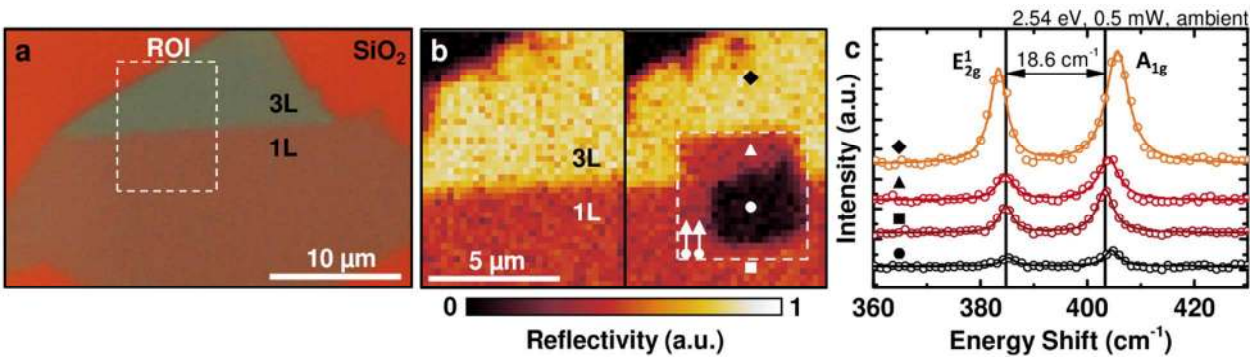

Figure 1. (a) Optical microscopy image (100x) of exfoliated single- (1L) and tri-layer (3L) MoS_2 on a Si/SiO_2 substrate. (b) Monochromatic reflectivity map of before (left) and after (right) a laser scan in the electrolyte of the ROI defined in (a). The arrows indicate scan direction. Step size 250 nm, dose 1 mW x 20 s at each spot. (c) Raman spectra of the spots marked in (b) of untreated, unaffected and photo-degraded regions.

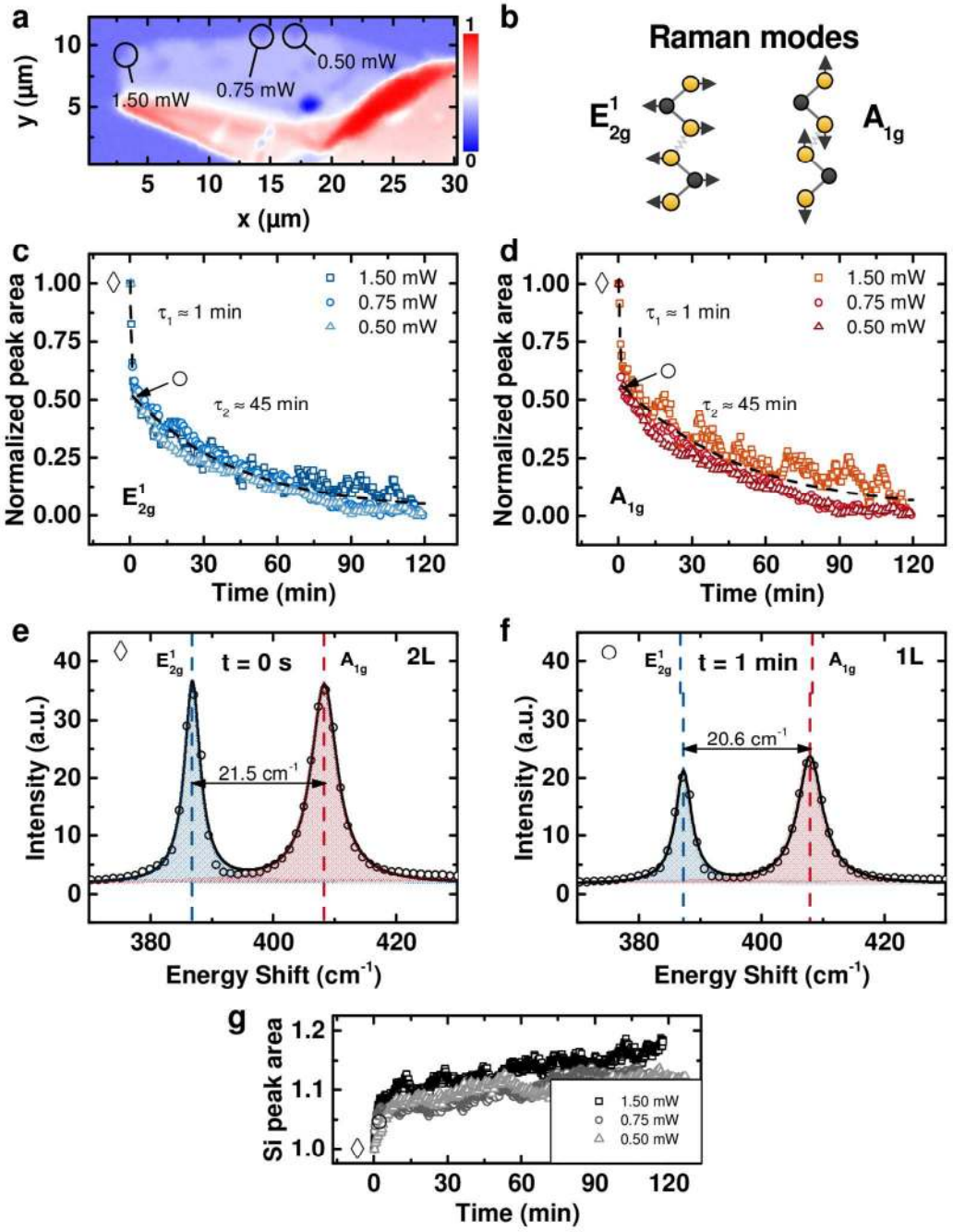

Figure 2. (a) Monochromatic reflectivity map of a MoS_2 bilayer sample after extensive photo-degradation measurements immersed in water (circles mark the corroded spots used for time-resolved measurements. More spots on the flake have been investigated). (b) Scheme of the direction of movement of Mo and S atoms for the two Raman active phonon modes E^1_{2g} and A_{1g}, respectively. (c) and (d) Normalized Raman peak area intensity of the E^1_{2g} (c) and A_{1g} (d) mode

of the spectra shown in (e) and (f) as a function of laser illumination time for the MoS_2 flake immersed in DI water for various light intensities. The fits show two different decay rates for the bilayer and the remaining monolayer-flake. (e) and (f) Raman spectra showing the E^1_{2g} and A_{1g} modes of an initial MoS_2 bilayer-flake (e) at the beginning of laser irradiation (◊) and (f) after degradation from bi- to a monolayer after 1 min (○). (g) Raman peak area intensity of the silicon TO-phonon mode that depicts the complementary increase of the Raman signal originating from the substrate.

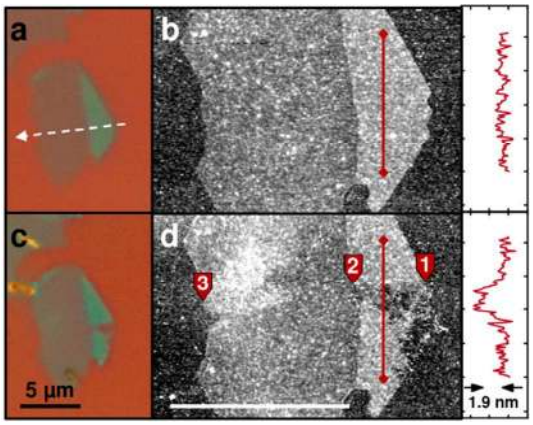

Figure 3. (a, c) Optical microscopy (100x) and (b, d) AFM image of exfoliated single- and trilayer flake on a Si/SiO_2 substrate before (top) and after (bottom) laser linescan immersed in electrolyte. The dashed arrow indicates the scan direction. The steps from substrate to trilayer (1), from trilayer to monolayer (2) and from monolayer to substrate (3) are highlighted with labels. Photo-degradation takes predominantly place on edge sites. The corresponding AFM height-profiles at the trilayer regions are depicted on the right (red lines). Scale bars 5 µm.

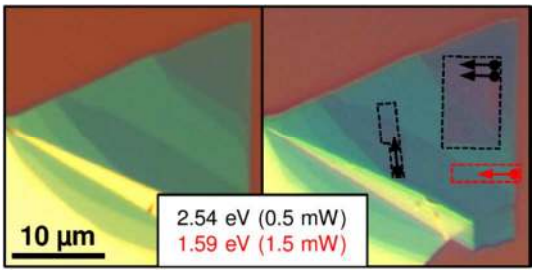

Figure 4. Optical microscopy image of a multi-layer MoS_2 flake before (left) and after (right) area illumination scans with a laser energy below (1.59 eV) and above (2.54 eV) the direct band gap, respectively. The MoS_2 flake is unaffected for exposure to light with energy smaller than the band-gap (red marked area). In case of illumination with energy larger than the band gap, corrosion of the MoS_2 flake is clearly visible (black marked areas). Scan parameters: step size 250 nm, illumination at each spot: 21 s.

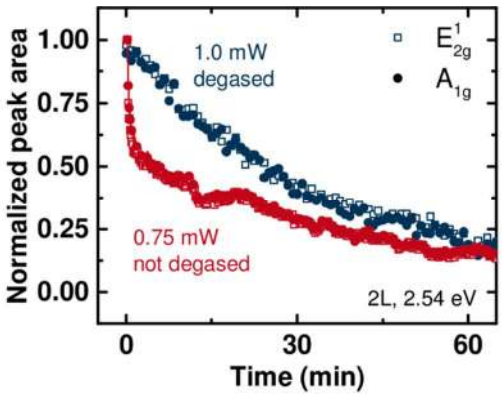

Figure 5. Normalized Raman peak area of the E^1_{2g} and A_{1g} mode as a function of laser illumination time on the edge site of a bilayer-flake. The upper curve (blue) corresponds to a flake immersed in water with reduced oxygen concentration in the electrolyte, the lower curve (red) to water with a natural amount of dissolved oxygen.